The Third *Swift* Burst Alert Telescope Gamma-Ray Burst Catalog

Amy Lien[1,2,†*]**,Takanori Sakamoto**[3,†]**, Scott D. Barthelmy**[4]**, Wayne H. Baumgartner**[1,2]**, Kevin Chen**[5]**, Nicholas R. Collins**[1,2]**, Jay R. Cummings**[4]**, Neil Gehrels**[4]**, Hans A. Krimm**[1,6]**, Craig. B. Markwardt**[4]**, David M. Palmer**[7]**, Michael Stamatikos**[8]**, Eleonora Troja**[1,9]**, Tilan N. Ukwatta**[10]

† *These authors contributed equally to this work.*

[1]*Center for Research and Exploration in Space Science and Technology (CRESST) and NASA Goddard Space Flight Center, Greenbelt, MD 20771, USA*

[2]*Department of Physics, University of Maryland, Baltimore County, 1000 Hilltop Circle, Baltimore, MD 21250, USA*

[3]*Department of Physics and Mathematics, College of Science and Engineering, Aoyama Gakuin University, 5-10-1 Fuchinobe, Chuo-ku, Sagamihara-shi, Kanagawa 252-5258, Japan*

[4]*NASA Goddard Space Flight Center, Greenbelt, MD 20771, USA*

[5]*Department of Physics, University of California, Berkeley, 366 LeConte Hall MC 7300, Berkeley, CA, 9472*

[6]*Universities Space Research Association, 10211 Wincopin Circle, Suite 500, Columbia, MD 21044, USA*

[7]*Los Alamos National Laboratory, B244, Los Alamos, NM, 87545, USA*

[8]*Department of Physics and Center for Cosmology and Astro-Particle Physics, Ohio State University, Columbus, OH 43210, USA*

[9]*Department of Physics and Department of Astronomy, University of Maryland, College Park, MD 20742, USA*

[10]*Space and Remote Sensing (ISR-2) and Physics Division (P-23), Los Alamos National Laboratory, Los Alamos, NM 87545, USA*

E-mail: amy.y.lien@nasa.gov

To date, the Burst Alert Telescope (BAT) onboard *Swift* has detected ~ 940 gamma-ray bursts (GRBs), within which close to 320 GRBs have redshift measurements, around 90 GRBs have burst durations (T_{90}) shorter than ~ 2 s, and about 75 bursts were found in ground processing. Here, we present the analyses of the BAT-detected GRBs for the past ten years. We report summaries of GRB characteristics from analyses using event data (i.e., data within approximately 250 s before and 950 s after the BAT trigger time), such as the burst refined positions, durations, and spectral analyses (spectral indices, fluxes, and fluences) using simple power-law and cutoff power-law fits. In addition, we perform searches for GRB emissions before or after the event data using the BAT survey data. We estimate the false detection rate and report a list of GRBs with confirmed extended emission beyond event data. When redshifts are available, we also investigate GRB properties with redshifts.

1. Introduction

Since *Swift* launched on Nov. 20, 2004, The Burst Alert Telescope (BAT) onboard *Swift* has detected 938 GRBs (until GRB150206A). There are two main trigger methods that BAT adopts: (1) the rate trigger criteria, which search for GRBs based on count rate increases in the light curves, and (2) the image trigger criteria, which discover bursts based on images created with different time intervals ($\gtrsim$ minute). For all the BAT-detected bursts, 720 are triggered by on-board rate triggers, 145 are triggered by on-board image triggers, and 73 are found later in ground analyses.

In this catalog, we analyze all the BAT GRBs observed in the past ten years. The main GRB characteristics (e.g., burst durations, spectral fits) are acquired from analyses using the event data, which record information of individual photons and usually cover ranges between ~ 250 s before and ~ 950 s after the BAT trigger time. In addition to studies using event data, we also search for possible extended emission beyond the event data range using the BAT survey data. The survey data are binned in ~ 5-min interval, and cover time periods that do not have event data.

2. Summary of the BAT observing time

Based on the BAT log files, BAT spends $\sim 78\%$ of the time performing observations and searching for GRBs. For the rest of the $\sim 22\%$, BAT cannot trigger a burst mainly due to (1) telescope slewing, which consists of $\sim 11\%$ of the mission time, and (2) high background counts when the telescope passes through the South Atlantic Anomaly (SAA), which covers another $\sim 11\%$ of the time. These fractions remain pretty stable throughout the years.

3. Characteristics of GRB prompt emissions

3.1 BAT event data analyses

All the BAT event data used in these analyses are downloaded from HEASARC[1]. We use the standard BAT software (HEASOFT 6.15[2]) and the latest calibration database (CALDB[3]) to perform analyses for event data.

For spectral analyses, we use the commonly adopted X-ray fitting package, XSPEC[4]. Following the second BAT GRB catalog [1], we fit the GRB spectra with two different models: simple power law (PL) and cutoff power law (CPL). The simple power-law model is described by the following equation,

$$f(E) = K_{50}^{\mathrm{PL}} \left(\frac{E}{50 \text{ keV}} \right)^{\alpha^{\mathrm{PL}}}, \tag{3.1}$$

where $f(E)$ is the photon flux at energy E. α^{PL} is the PL index, and K_{50}^{PL} is the normalization factor at 50 keV, with units of photons cm^{-2} s^{-1} keV^{-1}. The cutoff power-law model is expressed as,

$$f(E) = K_{50}^{\mathrm{CPL}} \left(\frac{E}{50 \text{ keV}} \right)^{\alpha^{\mathrm{CPL}}} exp\left(\frac{-E(2 + \alpha^{\mathrm{CPL}})}{E_{\mathrm{peak}}} \right), \tag{3.2}$$

---

*Speaker.

[1]http://heasarc.gsfc.nasa.gov/cgi-bin/W3Browse/swift.pl

[2]http://heasarc.nasa.gov/lheasoft/

[3]http://heasarc.gsfc.nasa.gov/docs/heasarc/caldb/swift/

[4]http://heasarc.gsfc.nasa.gov/xanadu/xspec/

where α^{CPL} is the CPL index, and K_{50}^{CPL} is the normalization factor at 50 keV, with units of photons cm^{-2} s^{-1} keV^{-1}.
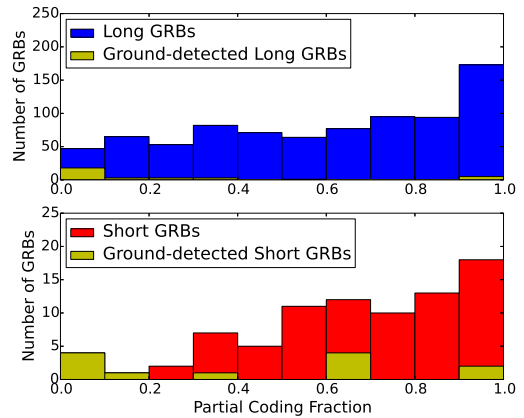
3.2 Results

The general characteristics of the BAT GRB prompt emissions remain similar to those previously reported in [1]. Figure 1 presents two main distributions of GRB prompt emissions. The left panel shows the distributions of burst durations (T_{90}, which is defined as durations that capture 90% of the burst emissions), and the right panel shows the hardness ratio versus T_{90}. About $\sim 10\%$ of BAT GRBs are short ($T_{90} \leq 2$ s), which is much less than the fraction observed in BATSE and Fermi/GBM [1, 2, 3]. In addition, the short GRBs in the BAT populations are slightly harder than the long GRBs.
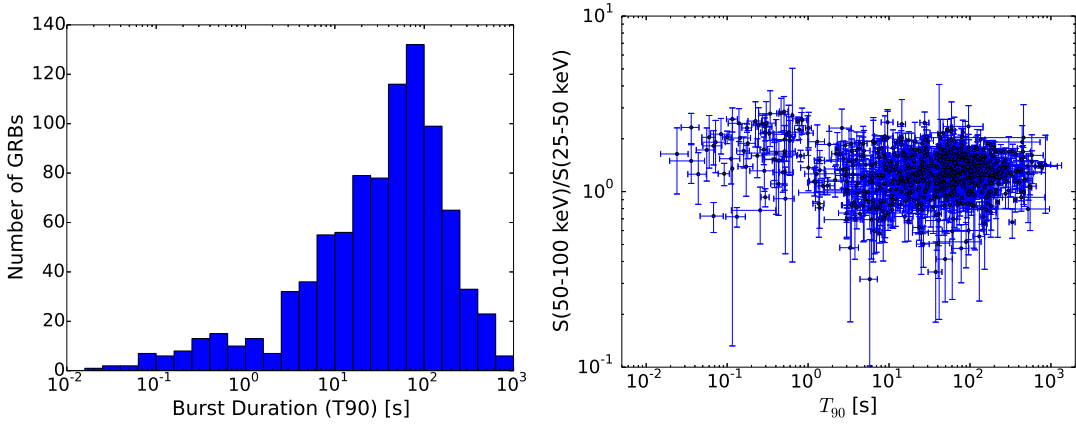
Figure 1: *Left panel*: The burst duration (T_{90}) distribution. The bin size of this plot is 0.2 in log scale. *Right panel*: Hardness ratio (i.e., fluence in 50-100 keV over fluence in 25-50 keV) versus T_{90}. The fluences are estimated using the best-fit models.

Figure 2 shows the partial coding distribution for both long and short GRBs. The partial coding fraction corresponds to the fraction of illuminated detector plane. In other words, it is related to the burst incident angle. An on-axis burst would have a partial coding fraction of one, while a $\sim 30^o$ and $\sim 50^o$ off-axis burst would have a partial coding fraction of ~ 0.7 and ~ 0.2, respectively.

The distribution of ground-detected bursts is marked in yellow. GRBs found during telescope slews are not included in this plot, because it is hard to define the partial coding fraction during telescope slews. As seen in the figure, the on-board triggers have never detected short bursts with incident angles larger than $\sim 50^o$.

Similar to results in [1], most of the GRB spectra in the BAT energy range can be well-fitted by the simple PL model, and show no significant improvement in the their fits when changing to the CPL model. We

Figure 2: Distributions of the partial coding fraction for both long and short GRBs.

3

therefore report results from the simple PL fit for all GRBs, and present results from the CPL fit only when the χ^2 from the CPL fit shows significant improvement over the simple PL fit. We adopt the same criteria as the one in [1] to determine when CPL fit is better. That is, when $\Delta\chi^2 \equiv \chi^2_{\mathrm{PL}} - \chi^2_{\mathrm{CPL}} > 6$, we report results from both fits. The left panel of Fig. 3 presents the distribution of photon index α^{PL} for GRBs fitted better with the simple PL model. Similar to the results seen in the right panel of Fig. 1, the short bursts shows slightly harder spectra on average. There are 180 GRBs fitted better with the CPL model, which suggests that the turn-over points in their spectra, E_{peak}, happen in the BAT energy range. Moreover, these bursts are likely to have smaller uncertainties in their spectra data, and thus the data are sufficient to distinguish the difference between the simple PL and CPL models. The E_{peak} distribution of these 180 GRBs are shown in the right panel of Fig. 3. The E_{peak} distribution for the BAT-detected GRBs peaks at ~ 71 keV, which is different than the distributions from GRBs detected by other instruments like BATSE [1, 4].
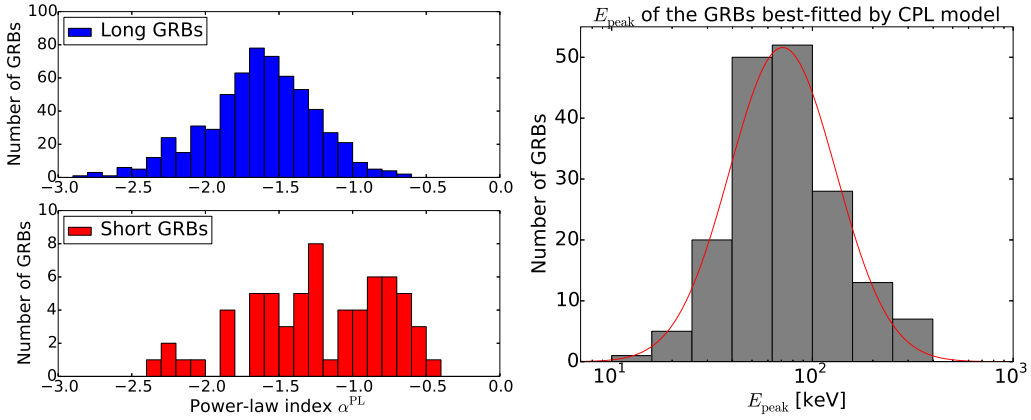
Figure 3: *Left panel*: Distributions of the GRB power-law indices α_{PL} for GRBs fitted better by the simple PL model. *Right Panel*: The E_{peak} distribution for GRBs fitted better with the CPL model.
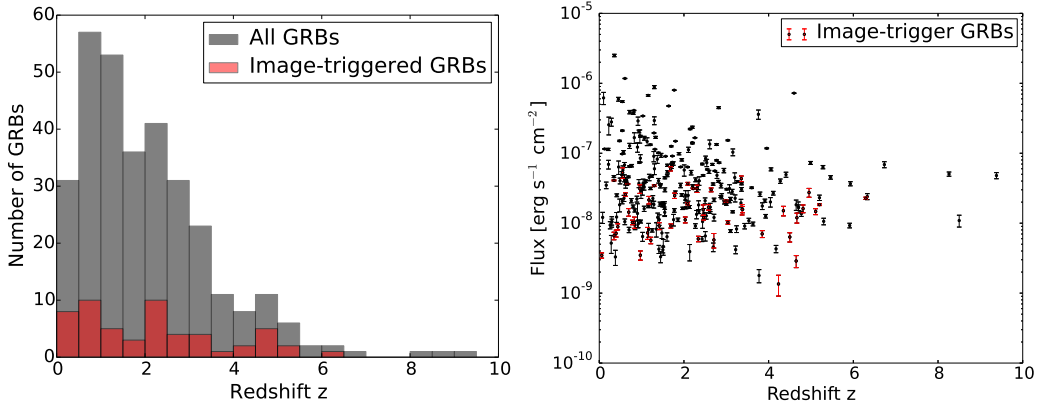
4. Redshift distributions

We summarize the redshift measurements for 317 BAT-detected GRBs. The information in this list is collected from and cross-checked between other online lists (e.g., GRBOX by Daniel Perley[5], online table by Nathaniel Butler[6]), the Gamma-ray Coordinates Network (GCN) circulars [5], and papers. The redshift list with full references will be included in the final catalog.

The redshift distribution of the BAT-detected GRBs is shown in the left panel of Fig. 4. The distribution of bursts found by image trigger is plotted in red. Compared to GRBs detected by rate triggers, the image-triggered GRBs are more uniformly distributed throughout all redshifts.

The GRB fluxes (15-150 keV) as a function of redshift is plotted in the right panel of Fig. 4. Again, the bursts found by image triggers are shown in red. As expected, image triggers generally find bursts with lower fluxes. There also seems to be a hint of missing population of low-flux GRBs close to the BAT's detection limit ($\sim 10^{-8}$ to 10^{-9} erg s^{-1} cm^{-2}) at high redshift ($z \gtrsim 5$). However, more high redshift GRB detections will be crucial to confirm (or exclude) this possibility.

---

[5]http://www.astro.caltech.edu/grbox/about.html

[6]http://butler.lab.asu.edu/swift/bat_spec_table.html

Figure 4: *Left panel*: GRB redshift distribution. *Right panel*: GRB fluxes (15-150 keV) from the best-fitted model as a function of redshift *z*.

5. Searching for GRB extended emissions

In additional to the event data analyses, we use the BAT survey data to perform a systematic search for possible GRB emissions beyond the ~ 1000 s event data range.

5.1 Survey data analyses

We use the result products of the 70-month survey analyses [6] to search for GRB extended emissions. [6] performs standard survey analyses using the script "batsurvey[7]", and generates mask-weighted, cleaned images for each observations in eight energy bands (14-20, 20-24, 24-35, 35-50, 50-75, 75-100, 100-150, 150-195 keV).

We select a sub-sample of these images that have time ranges within ~ 0.2 day before and ~ 1 day after the BAT trigger time. We then estimate the signal-to-noise ratios of the GRB locations in these images using the standard BAT analysis script "batcelldetect[8]". The GRB locations adopted here are reported by the X-Ray Telescope (XRT) on-board *Swift*. Note that because existing survey products only include data from Dec. 2004 to Aug. 2013, we only search through possible GRB emissions in survey data until Aug. 2013.

5.2 Quantifying false-detection rate

We perform a study of false-detection rate in order to find a reliable criterion to search for weak emission. To quantify the false detection rate, we estimate the signal-to-noise ratio using background locations around GRBs. We choose the background locations to be ~ 1 deg from the GRBs (so most of the time the background detections are from the same images as the GRB detections), and also ~ 1 deg from other x-ray sources. We adopt the x-ray source list from [7].

We quantify the false-detection rate R_{false} in a particular energy band with a specific signal-to-noise ratio threshold as follow,

$$R_{\text{false}} = \frac{\text{N}(> \text{SNR}_{\text{lim}})}{N_{\text{tot}}}, \tag{5.1}$$

---

[7]https://heasarc.gsfc.nasa.gov/ftools/caldb/help/batsurvey.html
[8]https://heasarc.gsfc.nasa.gov/ftools/caldb/help/batcelldetect.html

5

where $N(> SNR_{lim})$ is the number of survey images with the signal-to-noise ratios at the specific locations higher than the assigned threshold. N_{tot} is the total number of survey images we included in the search (i.e., the subset of all survey images that are close to GRB trigger times, as described above). Note that the image exposure times can vary from ~ 300 s to ~ 2500 s, with the majority of the exposure time around few hundred seconds. Ideally, one would require the observation time of each image to be identical to have a fair comparison of the signal-to-noise ratio in each image. However, because the survey process only produce one image for each observation, our estimation can only be based on these images with different exposure times. To produce survey images with finer time bins in each observation, one would need to re-process all survey data, which takes $\sim$ years to finish.

We quantify the false-detection rate for a range of different signal-to-noise ratio thresholds (from $\sim 2.0\sigma$ to $\sim 5.0\sigma$) in different energy bands. The energy ranges we tried include the eight bands used by the survey process (14-20 keV, 20-24 keV, 24-35 keV, 35-50 keV, 50-75 keV, 100-150 keV, 150-195 keV), an energy band covers the total range (14-195 keV), an energy band combines the three soft bands (14-35 keV), and an energy band that covers the three energy bands with higher effective area (35-100 keV).

Figure 5: The histogram of signal-to-noise ratios from the GRB background locations in 14-195 keV.
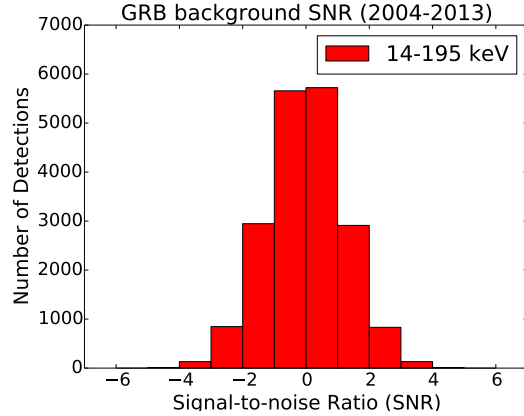
We investigate the expected detection rate for different criteria (i.e., different signal-to-noise ratios with different energy bands), and select some potentially useful criteria to perform further test by calculating the signal-to-noise ratios at the GRB locations. This give us a total number of real detections plus false detections at each GRB location. We search through each criterion until we find one that gives the largest ratio of the number of detections at the GRB location $N_{GRB\_locations}$ (i.e., number of real plus false detections) over the number of detections at the background locations $N_{bgd\_location}$ (i.e. false detections). In other words, we demand the ratio

$$r_{detect} \equiv \frac{N_{GRB\_locations}}{N_{bgd\_location}} = \frac{N(real + false)}{N(false)} \tag{5.2}$$

to be as large as possible. We find the criterion using images with energy band 14-195 keV and signal-to-noise ratio threshold above 4.3 sigma gives the highest r_{detect}. We thus adopt this criterion to search for possible emissions in survey data. With this criterion, we expect ~ 1 false detection in our search sample.

5.3 Results

We find 21 detections (16 GRBs) beyond the event data range, which are summarized in Table 1. Within these detections, 7 GRBs are previously classified as ultra-long GRBs, which are GRB121027A, GRB111215A, GRB111209A, GRB101225A, GRB100316D, GRB090417B, GRB060218 (e.g., [8]). Most of these detections happened after the BAT trigger times. However, there are two detections (GRB100316D and GRB101024A) occurred before the BAT trigger times.

Note that there are two detections (GRB060218 and GRB050730) happens within 500 sec after the BAT trigger times. This is because at earlier mission time, BAT downlinked a shorter range of event data that only covers until ~ 300 s after trigger time. Therefore, these two detections would have been covered by event data range if the GRBs occurred more recently. Also, GRB080319B is the well-known naked-eye burst [9]. It is possible that the extraordinary brightness of this burst is the main reason for the event being detectable for a long time in BAT. Thus, one needs to be cautious when exploring potential physical causes of these late time BAT detections, particularly for brighter GRBs in our sample.

Table 1: Lists of GRBs detected in survey data with signal-to-noise ratio $> 4.3\sigma$ in 14-195 keV. We expect on average ~ 1 false detection in our search sample.

GRB name	detection time (since T0) [s]	image exposure time [s]	SNR in 14-195 keV
GRB121027A	1327.45	496.0	19.32
GRB121027A	5351.45	732.0	11.64
GRB111215A	703.0	840.0	12.27
GRB111209A	4814.0	2600.0	40.98
GRB111209A	10606.0	2584.0	14.08
GRB111209A	16427.0	2400.0	7.58
GRB111209A	565.0	630.0	92.73
GRB101225A	1372.0	300.0	10.28
GRB101225A	4936.0	2601.0	4.55
GRB101024A	-5252.13	779.0	4.73
GRB100728A	981.73	792.0	4.83
GRB100316D	-775.0	600.0	9.01
GRB091127	5192.90	409.0	4.36
GRB090417B	662.0	1140.0	23.51
GRB090404	44356.93	557.0	4.31
GRB090309	4075.176	2400.0	4.40
GRB080319B	938.1	799.0	11.26
GRB070518	57158.83	1381.0	4.92
GRB070419B	3724.13	2400.0	5.22
GRB060218	404.0	2327.0	19.20
GRB050730	356.2	390.0	8.53

We further compare these late-time emissions to the *Swift*/XRT light curves generated by the Burst Analyser[9] [10, 11, 12]. The Burst Analyser can plot the GRB light curves from both the BAT event data and the XRT data in the 15-50 keV range. The equivalent XRT fluxes in the 15-50 keV range are estimated by extrapolating the XRT spectrum in 0.3-10 keV. We also calculate the BAT fluxes in the 15-50 keV range with the BAT spectra generated from the survey data. Figure 6 shows two examples comparing the BAT detections in the survey data with observations from the BAT event data and the XRT data. Results show that from most of the late-time detections in the survey

---

[9]http://www.swift.ac.uk/burst_analyser/

data, the BAT extended emissions generally follow the behavior seen in the XRT light curves, and the photon indices from the simple PL fit (α^{PL}) are similar to the one derived from the XRT data.
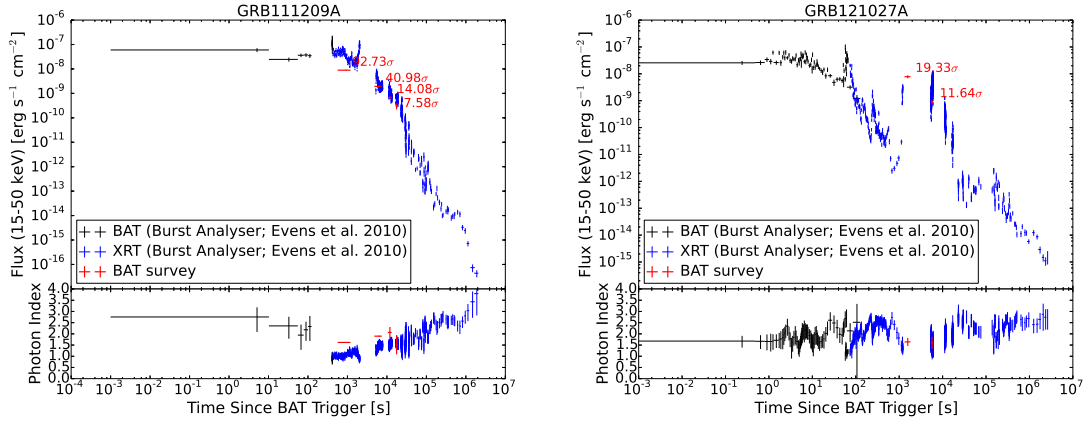
Figure 6: Examples of comparisons between detections in the BAT survey data, BAT event data, and the XRT data.

6. Conclusions

We present summaries of the event data analyses for BAT-detected GRBs for the past ten years, including burst durations, spectral characteristics, BAT triggering methods, and a compiled redshift list. Furthermore, we report a list of GRB extended emissions detected in the survey data. The full results and tables will appear in the complete version of the third BAT GRB catalog.

References

[1] T. Sakamoto, S. D. Barthelmy, W. H. Baumgartner et al., *The Second Swift Burst Alert Telescope Gamma-Ray Burst Catalog*, ApJS **195** (2011) 2

[2] W. S. Paciesas, C. A. Meegan, G. N. Pendleton et al., *The Fourth BATSE Gamma-Ray Burst Catalog (Revised)*, ApJS **122** (1999) 465

[3] A. von Kienlin, C. A. Meegan, W. S. Paciesas, et al., *The Second Fermi GBM Gamma-Ray Burst Catalog: The First Four Years*, ApJS **211** (2014) 13

[4] A. Goldstein, R. D. Preece, R. S. Mallozzi et al., *The BATSE 5B Gamma-Ray Burst Spectral Catalog*, ApJS **208** (2013) 21

[5] S. D. Barthelmy, P. Butterworth, T. L. Cline et al., *BACODINE, the Real-Time BATSE Gamma-Ray Burst Coordinates Distribution Network*, APSS **231** (1995) 235

[6] W. H. Baumgartner, J. Tueller, C. B. Markwardt, et al., *The 70 Month Swift-BAT All-sky Hard X-Ray Survey*, ApJS **207** (2013) 19

[7] H. A. Krimm, S. T. Holland, R. H. D. Corbet, et al., *The Swift/BAT Hard X-Ray Transient Monitor*, ApJS **209** (2013) 14

[8] A. J. Levan, N. R. Tanvir, R. L. C. Starling, et al., *A New Population of Ultra-long Duration Gamma-Ray Bursts*, ApJ **781** (2014) 13

[9] J. L. Racusin, S. V. Karpov, M. Sokolowski, et al., *Broadband observations of the naked-eye γ-ray burst GRB080319B*, NATURE **455** (2008) 183

[10] P. A. Evans, R. Willingale, J. P. Osborne, et al., *The Swift Burst Analyser. I. BAT and XRT spectral and flux evolution of gamma ray bursts*, A&A **519** (2010) 102

[11] P. A. Evans, A. P. Beardmore, K. L. Page, et al., *Methods and results of an automatic analysis of a complete sample of Swift-XRT observations of GRBs*, MNRAS **397** (2009) 1177

[12] P. A. Evans, A. P. Beardmore, K. L. Page, et al., *An online repository of Swift/XRT light curves of ?-ray bursts*, A&A **469** (2007) 379

PoS(SWIFT 10)038